



# Particle distribution and velocity in electrokinetically induced banding

Massimiliano Rossi<sup>1</sup> · Alvaro Marin<sup>2</sup> · Necmettin Cevheri<sup>3</sup> · Christian J. Kähler<sup>1</sup> · Minami Yoda<sup>3</sup>

Received: 22 January 2019 / Accepted: 18 March 2019  
© Springer-Verlag GmbH Germany, part of Springer Nature 2019

## Abstract

Colloidal particles may be repelled from/attracted to the walls of glass micro-channels when an electro-osmotic flow is combined with a Poiseuille flow. Under certain conditions, the particles assemble into bands after accumulating near the walls (Cevheri and Yoda in *Lab Chip* 14(8):1391–1394, 2014). The fundamental physical mechanisms behind these phenomena remain unclear and up to now only measurements within 1  $\mu\text{m}$  of the walls have been available. In this work, we applied a 3D particle-tracking technique, astigmatism particle tracking velocimetry, to measure the concentration and velocity distribution of particles across the depth of the entire micro-channel. The experiments show that the particles are depleted in the bulk as they become concentrated near the bottom and top walls and this particle redistribution depends strongly upon the bulk particle concentration. The results suggest that bands form in a region where particles are practically immobile and their volume fraction increases at least an order of magnitude with respect to the original volume fraction. Our results suggest that particle accumulation and band formation near the walls may be triggered by forces generated in the bulk since the banding and particle accumulation extends at least a few  $\mu\text{m}$  into the channel, or at length scales beyond the range of surface forces due to wall interactions.

**Keywords** Electrokinetic banding · Electro-osmotic flow · Micro/nanoparticles · Self-assembly · Astigmatic-PTV · Micro-PIV

## 1 Introduction

Transport of microparticles suspended in an aqueous electrolyte solution through sub-millimeter conduits is not only a technological challenge, but is also an important research area in colloid science and fluid dynamics. It is well known that solid surfaces acquire electrical charges when submerged in water. Such charged surfaces develop electrical double layers (EDL) that extend into the bulk liquid over distances that are of the order of 10 nm for glass channels

and electrolyte solutions at low concentration ( $\sim 1$  mM). Although such length scales may seem small, especially when compared with typical diameters of microfluidic channels (tens of micrometers), the presence of EDLs can have a profound effect on the spatial distribution of particles in the bulk of the flow.

The equilibrium distribution of mobile charges near charged surfaces is a classical problem which yields exact solutions for simple geometries, under the assumption that the ions and particles only move as a consequence of Brownian motion and their electrostatic interactions (Russel et al. 1989; Lyklema 1991). Such equilibria can be easily disturbed by applying an external electrical field parallel to the surface. In that case, the applied electric field induces a liquid motion relative to the stationary charged surface. Such a flow is known as electroosmotic (EO) flow (Anderson 1989; Kirby and Hasselbrink 2004; Sadr et al. 2004; Bruus 2008). Although EO flows are used in microfluidics for a variety of applications (Manz et al. 1994; Schasfoort 1999), the electric field also affects the motion of any colloidal particles suspended in the flow.

---

**Electronic supplementary material** The online version of this article (<https://doi.org/10.1007/s10404-019-2227-9>) contains supplementary material, which is available to authorized users.

---

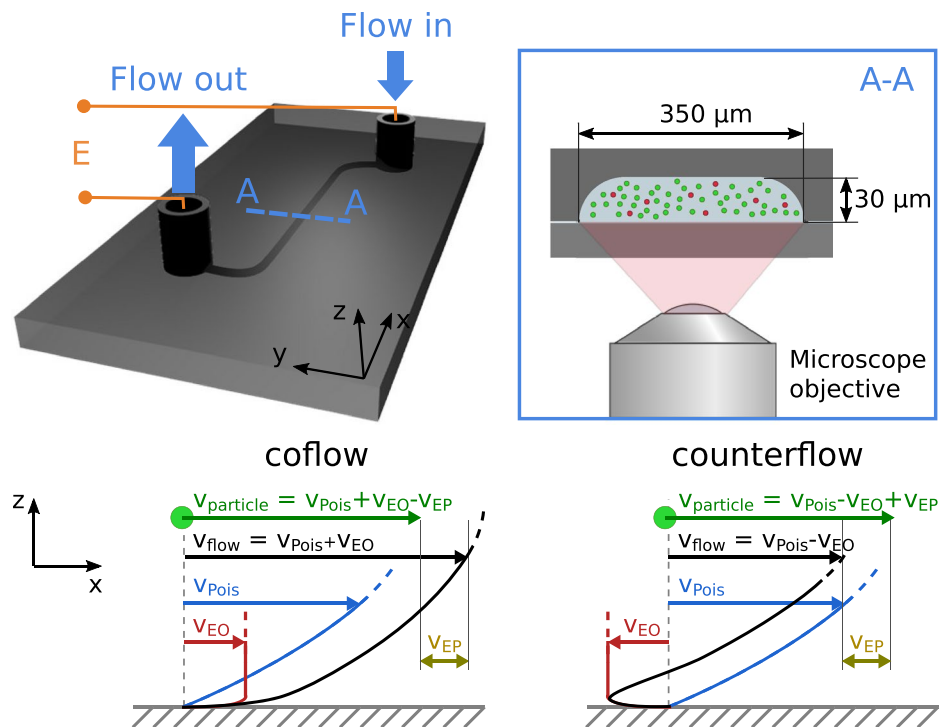
✉ Massimiliano Rossi  
rossi@fysik.dtu.dk

<sup>1</sup> Institute of Fluid Mechanics and Aerodynamics, Bundeswehr University Munich, 85577 Neubiberg, Germany

<sup>2</sup> Physics of Fluids, University of Twente, 7522 NB Enschede, The Netherlands

<sup>3</sup> G. W. Woodruff School of Mechanical Engineering, Georgia Institute of Technology, Atlanta, GA 30332-0405, USA

**Fig. 1** (Top) schematic of the microfluidic devices: the inlet and outlet are connected to electrodes to induce a potential difference across the micro-channel. In the inset, the trapezoidal micro-channel cross section of depth  $30\ \mu\text{m}$  and width  $350\ \mu\text{m}$  is shown. The fluid is seeded with PS spheres labeled with different colors and observed from below through an inverted microscope. (Bottom) sketch of the velocity profiles. We term EO and Poiseuille flows in the same direction “coflow,” and EO and Poiseuille flows in the opposite direction “counterflow.” The particles’ velocity results from the combination of the fluid flow (Poiseuille and EO flows) and particle electrophoresis



One of the main concerns in EO flow of colloidal suspensions is the spatial distribution of the particles themselves. It has been shown experimentally (Cevheri and Yoda 2014a, c) that dielectric colloidal particles, which also acquire a surface charge when exposed to an aqueous electrolyte solution, are repelled from a charged channel surface when a combined EO flow and Poiseuille flow is established, with both flows driven in the same direction by an electric field and a pressure gradient, respectively (Fig. 1 “coflow”). Kim and Yoo (2009) exploited this phenomenon to focus and separate particles in a flow, while Arca et al. (2015) reported transverse migration of DNA molecules in capillary electrophoresis with a concurrent pressure gradient. On the other hand, when the EO and Poiseuille flows are in opposite directions (Fig. 1 “counterflow”), it has been shown by Cevheri and Yoda (2014a) that the opposite effect occurs: particles are attracted towards, and accumulate near, the channel surface. Such an effect was studied experimentally using evanescent wave velocimetry, probing the first  $\mu\text{m}$  of the flow next to the surface (Cevheri and Yoda 2014a; Yee and Yoda 2018). A similar “cross-stream” migration was reported by Li and Xuan (2018) in a straight channel with a contraction and expansion at the inlet and outlet, respectively.

Surprisingly, for electric field magnitudes  $|E|$  above a critical value  $|E_{\text{min}}|$ , the accumulated particles near the wall assemble into concentrated streamwise bands (Cevheri and Yoda 2014a, b). The particles in the bands appear to be in a liquid-like (*vs.* solid-like) state—i.e., particles show no

distinct order—and the bands show reversibility and reproducibility (Cevheri and Yoda 2014a, b).

Previous research has been performed using evanescent-wave illumination to analyze regions close to the channel surface or wall (typically  $< 1\ \mu\text{m}$ ) (Cevheri and Yoda 2014a, b, c). At present, the mechanisms for particle depletion/accumulation and banding formation remain unresolved. Moreover, nothing is known to this date on the particle distribution and particle velocities in the bulk of the flow beyond the region illuminated by evanescent waves. Such measurements could clarify where the maximum particle concentration occurs, and help us understand if we are dealing with near-wall short-range forces, or intermediate-range forces, such as the “dielectrophoretic-like” lift force due to an applied electric field (Yariv 2006), and the electroviscous force.

It may be possible that bands assemble due to an electrokinetic (EK), or electrohydrodynamic, instability caused by spatial gradients in the electrical properties of the fluid normal to the channel surface (Baygents and Baldessari 1998). The accumulation of particles near the surface can create a gradient in the electrical permittivity and conductivity normal to the wall, and hence the direction of the electric field (Navaneetham and Posner 2009). Previous EK stability analyses (Chang et al. 2009) suggest that the combination of (weak) shear flow and an applied electric field leads to the formation of counterrotating vortices, or “convection cells”; such an array of streamwise vortices could “sweep” the particles, once they accumulate near the surface, into band-like structures. Alternatively, band assembly may be

driven by interparticle interactions, which would likely only become significant once the particles are in close proximity (i.e., when a critical number of particles are concentrated near the bands).

To clarify and, if possible, distinguish between these hypotheses, in the present work we measure the particle distribution and velocity field over the entire channel cross section for typical cases where: (1) particles are repelled from, and depleted near the wall (coflow). (2) Particles are attracted to, and accumulate near the wall (counterflow at  $|E| < |E_{\min}|$ ). (3) Particles assemble into bands (counterflow at  $|E| > |E_{\min}|$ ). The measurements are performed using a 3D particle-tracking technique, namely the astigmatic particle tracking velocimetry (APTV) (Cierpka et al. 2010a, b; Rossi and Kähler 2014) and standard epifluorescence microscopy.

## 2 Materials and methods

**Microfluidic device** Combined Poiseuille and EO flow was established in a micro-channel having a  $350 \mu\text{m} \times 30 \mu\text{m}$  trapezoidal cross section and a total length of 47 mm (see Fig. 1). The micro-channel was manufactured using wet etching of a fused silica substrate. A solution of sodium tetraborate ( $\text{Na}_2\text{B}_4\text{O}_7$ ) in ultrapure water at a molar concentration of 1 mM was used as working fluid. The EO flow was driven by applying an electric potential difference at the inlet and outlet using platinum electrodes and a dc power supply. The  $\zeta$  potential of the fused-silica walls, measured following the procedure described in (Cevheri and Yoda 2013), was  $\zeta_w \approx -100$  mV. The Poiseuille flow was established by feeding fluid into the channel at a constant flow rate with a syringe pump (PHD 2000, Harvard Apparatus).

The suspended colloidal particles were fluorescent polystyrene (PS) spheres with radius (mean  $\pm$  standard deviation)  $a = 245 \pm 7.5$  nm. Since the particle concentration required for the experiments was too large for the APTV method (due to particle image overlapping), we used a mixture of particles with identical properties but labeled with different colors. Red-fluorescent particles (F8812, Life Technologies) at lower concentration ( $10^{14}$  particles/ $\text{m}^3$ ) were used for particle tracking, and green-fluorescent particles (F8813, Life Technologies), “invisible” to the camera, were used to achieve the required particle concentration. Both types of particles have the same  $\zeta$  potential of  $\zeta_p \approx -50$  mV (Cevheri and Yoda 2014a, c).

**Experimental conditions** The choice of the experimental conditions was based on previous studies (Cevheri and Yoda 2014a) to have depletion, accumulation and banding of particles. In particular, we chose a fixed particle number density  $c_\infty \approx 10^{16} \text{ m}^{-3}$  (volume fraction  $\phi \approx 0.05\%$ ), and a fixed flow rate of 100  $\mu\text{l/h}$  yielding a maximum velocity  $v^* = 5.2 \text{ mm/s}$  and a near-wall shear rate<sup>1</sup>  $\dot{\gamma} = 690 \text{ s}^{-1}$ .

Coflow with  $E = 21.3 \text{ V/cm}$  and counterflow with  $E \leq 63.8 \text{ V/cm}$  to have particle depletion (coflow), accumulation (counterflow with  $E < 42.6 \text{ V/cm}$ ) and banding (counterflow with  $E > 42.6 \text{ V/cm}$ ). The corresponding EO flow velocities induced by these electric fields— $0.14\text{--}0.43 \text{ mm/s}$  for  $E = 21.3\text{--}63.8 \text{ V/cm}$ —are much smaller than the Poiseuille flow velocities. Note also that the electric field induces a particle electrophoretic (EP) motion which is in the opposite direction as the EO flow, since the particles are negatively charged. The magnitude of the EP velocity is approximately half of the EO flow velocity. The final particles’ velocity results from the contribution of flow velocity and EP motion,  $v_{\text{particle}} = v_{\text{Pois}} \pm v_{\text{EO}} \mp v_{\text{EP}}$  (see also sketch in Fig. 1).

**3D particle tracking** The three-dimensional positions and velocities of the particles were obtained using APTV (Cierpka et al. 2010a, b; Rossi and Kähler 2014). The micro-channel was placed on the stage of an inverted epifluorescent microscope (Axio Observer Z1, Zeiss AG) and sequences of digital images of the particles in the flow were taken at 500 Hz, with an exposure time of 150  $\mu\text{s}$ , using a high-speed camera (Imager HS, LaVision). The optics consisted of a  $64\times$  microscope objective (Zeiss AG) and a cylindrical lens with 75 mm focal length placed in front of the camera sensor. The cylindrical lens introduces an astigmatic aberration which deforms the particle images in a systematic fashion depending on their position along the optical axis, or their depth position. The shape of a particle image together with the position of its center are used to retrieve the three-dimensional position of the corresponding particle. For more details about the measurement principle, see Rossi and Kähler (2014). The particles were illuminated with a green diode-pumped laser at wavelength  $\lambda = 532 \text{ nm}$ , close to the excitation wavelength of the red-fluorescent particles (Ex/Em 530 nm/607 nm). A longpass filter was used in the imaging system to ensure that only the light excited from the red fluorescent particles was recorded by the camera.

A typical APTV image is shown in Fig. 2a for a case in which no banding was present. The particle images show the characteristic elliptical shape with different sizes and orientations depending on their depth position. Note that the red particles in this experiment, which are the only particles visible in this image, are about 1% of the total (green and

<sup>1</sup> Note that different shear rates could yield different particle distributions and therefore different forces. The value of such forces could in principle be obtained assuming that the particles are distributed following Boltzmann distributions. However, this implies that particles are in thermodynamic equilibrium, which is clearly not the case in our experiments. For that reason, we decide to restrict these studies to a single shear rate and explore the particle distribution in depth. Analysis and discussion on the effect of different shear rates can be found in recent publications (Yee and Yoda 2018).

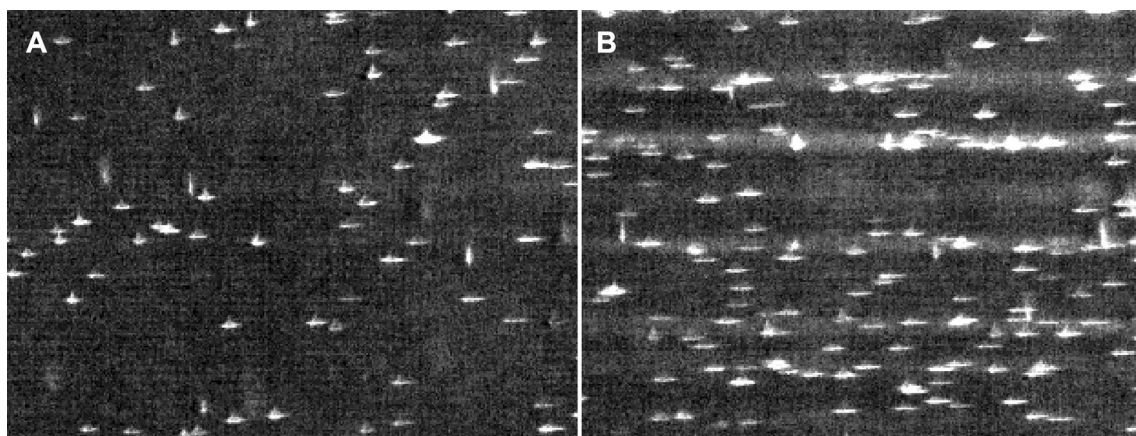


**Fig. 2** Particle images obtained with astigmatic optics (63× microscope objective and cylindrical lens in front of the camera sensor). Particle images of different shapes correspond to particles at different depth position within a depth of  $\sim 7\ \mu\text{m}$ . Flow is from left to right

red) particles. When the banding occurs, the bands are visible as faint background stripes (Fig. 2b), most likely due to scattering of the light emitted by the red particles inside the bands and the weak emission from green particles.

### 3 Results

**Velocity and concentration profiles** Results of the APTV measurements for coflow at  $E = 21.3\ \text{V/cm}$ , Poiseuille flow at  $E = 0\ \text{V/cm}$ , and counterflow at  $E = 42.6\ \text{V/cm}$  are shown in Fig. 3 (see also the corresponding movie in the Online Resource 1). The depth of the measurement volume using the 64× objective was about  $7\ \mu\text{m}$  so that five vertical scans were necessary to cover the entire channel height. Overall, the measurements cover a volume of  $180\ \mu\text{m} \times 200\ \mu\text{m} \times 30\ \mu\text{m}$  located at the central part of the micro-channel. As shown in Fig. 3, the particles in a pure Poiseuille flow are uniformly distributed across the channel height. For the coflow case, however, they are strongly depleted from the wall, and for the counterflow case, the particles are strongly concentrated near the top and bottom walls and depleted in the bulk. Note that the lower particle concentration at the top wall is actually a measurement artifact: measurements taken close to the top wall have greater background noise due to a higher number of out-of-focus particle images (we image through the bottom of the channel), reducing the number of valid particle measurements there.

Due to the large aspect ratio (11.7) of the channel cross section, we can assume that the flow in the measurement volume away from the side walls is two dimensional and plot the velocities and concentration only as a function of  $z$ . The velocity profiles for the three cases in Fig. 3, obtained

and initial bulk particle concentration is identical in both cases. **a** Counterflow at  $E = 21.3\ \text{V/cm}$ : no bands are formed. **b** Counterflow at  $E = 42.6\ \text{V/cm}$ : particles accumulate in bands aligned along the streamwise direction

from a total of 1000 image recordings, are shown on the top row of Fig. 4. In particular, we achieved an average of 100–200 valid points for each image recording, depending on the different cases. The velocities were calculated using a nearest-neighbor particle tracking scheme, with particles in one frame paired with particles in the subsequent frame. The main sources of error in the data are due to small fluctuations of the flow rate around the mean value and uncertainties

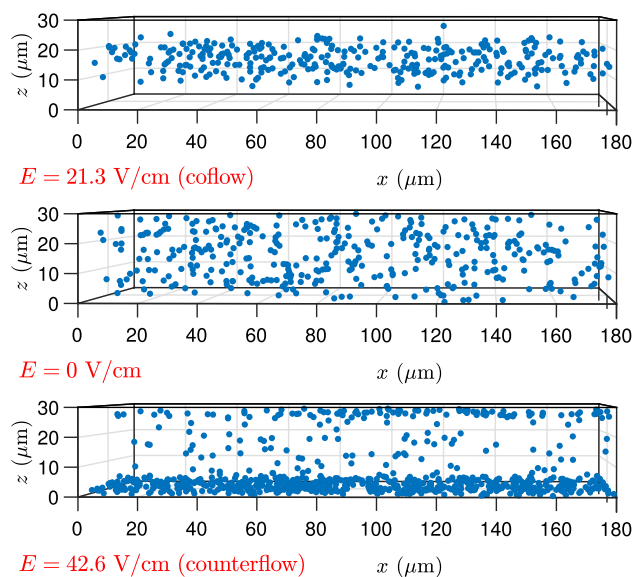


**Fig. 3** Position of tracer particles inside the channel as measured by APTV (see also animation in the Online Resource 1). The direction of the Poiseuille flow is from left to right. For pure Poiseuille flow the particles are evenly distributed in the channel. For coflow, the particles accumulate in the bulk and are depleted near the walls; for counterflow, the particles accumulate near the walls and are depleted in the bulk



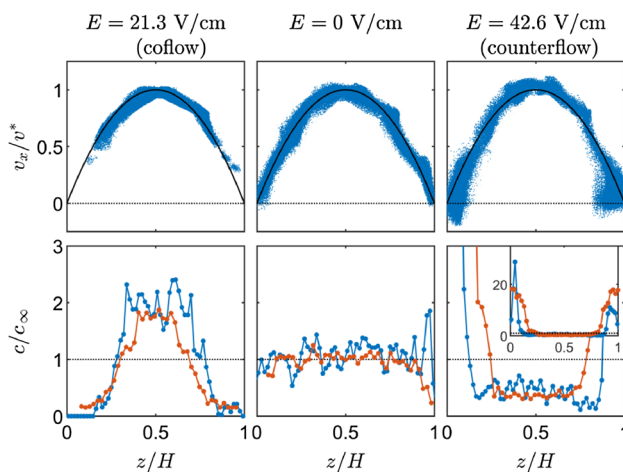


**Fig. 4** Velocity and concentration profiles for coflow at  $E = 21.3$  V/cm, Poiseuille flow at  $E = 0$ , and counterflow at  $E = 42.6$  V/cm. Velocities are normalized with the maximum velocity  $v^*$  in the pure Poiseuille flow and concentrations are normalized with the average concentration  $c_\infty$  measured for a reference experiment without flow. The blue and the red lines in the concentration profiles represent the results obtained from APTV and conventional segmentation measurements, respectively. The EO flow is not strong enough to affect significantly the velocity profiles. For coflow, particles deplete from the walls and accumulate in the center of the channel with a concentration of about  $2c_\infty$ . For counterflow, particles accumulate at the wall with a concentration 30 times larger than  $c_\infty$  (as shown in the inset) and deplete from the center to approximately half of  $c_\infty$  (color figure online)

in determining the position along the  $z$ -direction around  $\pm 0.2 \mu\text{m}$  (the uncertainty in determining position along the  $x$ - and  $y$ -directions is about one order of magnitude less). In general, the velocity profiles do not deviate significantly from the pure Poiseuille flow profile, as expected due to the relative low magnitude of the EO flow and EP migration. For coflow at  $E = 21.3$  V/cm, no data are obtained near the wall because there are few tracer particles there. For counterflow at  $E = 42.6$  V/cm, the particles are concentrated near the wall, and both positive and negative velocities are observed near the wall fluctuating around 0.

The concentration profiles are calculated counting the number of particles in bins with a width of  $0.5 \mu\text{m}$ . The concentration value of each bin is then normalized versus the corresponding value obtained in a reference experiment with particles evenly distributed (so that a value of 1 corresponds to  $c_\infty$ ). Results are shown in the second row of Fig. 4. A uniform concentration profile is observed for  $E = 0$  as expected. For  $E = 21.3$  V/cm, the particles are strongly depleted from the wall and accumulate in the center of the channel with a concentration  $\approx 2c_\infty$ . The opposite behavior is observed for  $E = 42.6$  V/cm, where the concentration is  $c \approx 0.4c_\infty$  in the center and  $c \approx 30c_\infty$  close to the wall (as shown in the inset at the bottom wall where the measurement is more accurate). The concentration values close to the walls are in agreement

with what previously observed in Cevheri and Yoda (2014a, c). In those studies, however, the measurements were limited to  $1 \mu\text{m}$  from the wall and it was hypothesized that the particle concentration returns quickly to  $c_\infty$  as moving toward the center, assuming that the particle accumulation/depletion is essentially a near-wall phenomenon. The present measurements show clearly that accumulation/depletion occurs across the whole channel depth.

In comparison with conventional segmentation approaches, APTV measurements allow to measure concentration profiles with a better resolution. In Fig. 4 (red line) we reported the same concentration profiles measured with a traditional segmentation approach. Specifically, microscopy images were taken with the  $64\times$  objective (without cylindrical lens), scanning through the micro-channel depth with steps of  $0.67 \mu\text{m}$ . For each image (corresponding to a specific  $z$ -position), the in-focus particles were counted and normalized with the corresponding particles in the reference case (particles evenly distributed). Due to uncertainty in identifying in-focus particles (in this case around  $2 \mu\text{m}$ , an order of magnitude larger than for the APTV measurement), a significant averaging error in regions with large concentration gradient is present. Outside these regions, the segmentation and APTV results are in excellent qualitative and quantitative agreement.

**Particle concentration during banding** As reported earlier, particle banding occurs only above a certain threshold value of the electric field magnitude. To observe if band formation affects the particle concentration profiles, we measured the particle concentration profiles for four counterflow cases, two cases in which the bands were not yet present ( $E = 8.5$  V/cm and  $21.3$  V/cm) and two cases in which the bands were present ( $E = 42.6$  V/cm and  $63.8$  V/cm). The results are shown in Fig. 5. The particle concentration profiles were calculated using finer bins with widths of  $0.2 \mu\text{m}$ . For all values of  $E$ , the particles are concentrated within about 6 particle diameters from the wall, with a maximum concentration at about 3 particle diameters. The maximum concentrations increase linearly with  $E$  as shown in the inset of Fig. 5. From a qualitative point of view, the concentration profiles look alike regardless of the presence of bands.

On the other hand, the presence of bands should significantly affect the particle concentration profiles measured along the spanwise direction,  $y$ . Previous studies using evanescent-wave illumination have already confirmed that the particles assemble into bands within  $1 \mu\text{m}$  of the wall under appropriate conditions (Cevheri and Yoda 2014b). The current APTV measurements, however, show that the bands extend at least 6 particle diameters from the wall. This is shown in Fig. 6, where the particle concentration profiles along the spanwise direction are calculated for three different layers (including respectively particles between 4–6, 6–8 and 8–10 particle diameters from the wall). For the case with

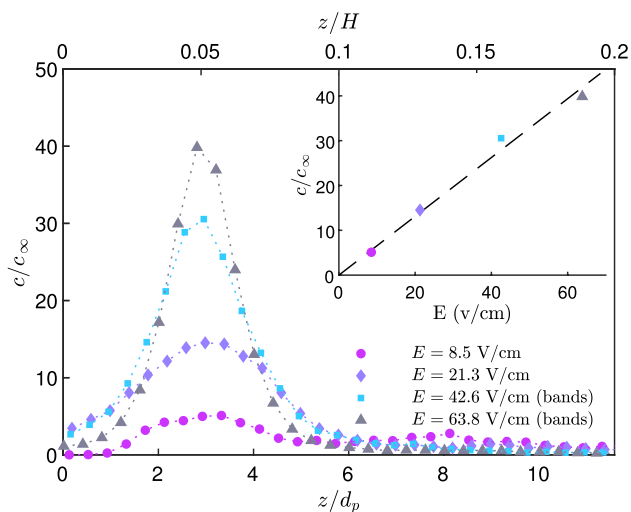


**Fig. 5** Concentration profiles for different electric fields (counterflow). Over the entire range of  $E$ , particles are concentrated in a region within 6 particle diameters of the wall, with a maximum concentration at about 3 particle diameters. Note that the extent of the accumulation region is independent of the presence of bands. In the inset, the maximum concentration is shown as a function of the electric field magnitude and appears to increase linearly with  $E$

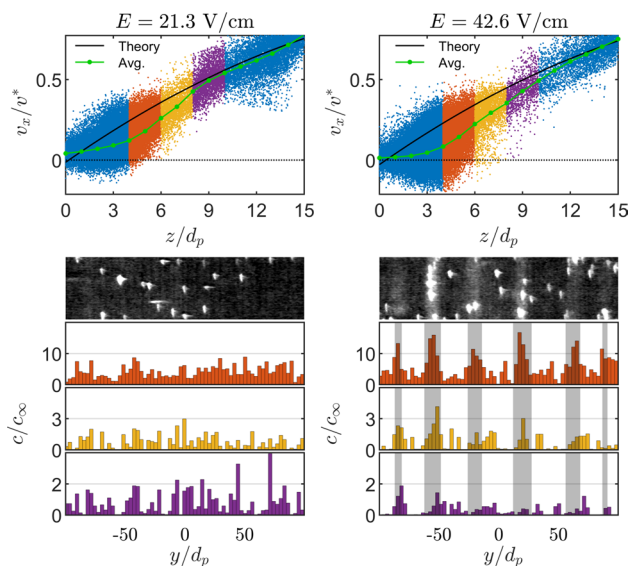


**Fig. 6** (Top) particles' velocity as a function of  $z$  for a case with no banding (counterflow with  $E = 21.3$  V/cm) and with banding (counterflow with  $E = 42.6$  V/cm). For both cases, a larger dispersion of the velocity data is observed in the region where the particles accumulate, showing that a larger amount of particles tends to “stop” in this region ( $z < 6$  particle diameters). (Bottom) particle concentration along the  $y$ -direction for different layers corresponding to 4–6, 6–8, 8–10 particle diameters from the wall. The color coding corresponds to the different layers. The channel center is at  $y/d_p = 0$ . For the case with no banding, the distribution of particles appears to be random. For the case with banding, a clear accumulation of particles in the regions where the bands are located (highlighted in gray) can be observed up to 6 particle diameters from the wall (color figure online)

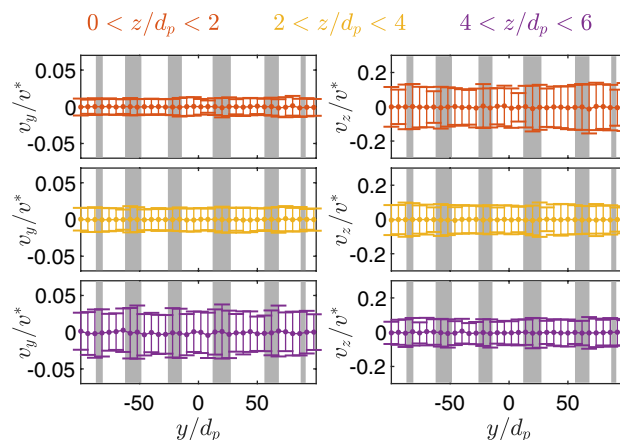


**Fig. 7** Average cross-stream particle velocities ( $v_y$  and  $v_z$ ) with error bars during banding (counterflow;  $E = 42.6$  V/cm) along the  $y$ -direction for different layers corresponding to 0–2, 2–4, and 4–6 particle diameters from the wall. The channel center is at  $y/d_p = 0$ . The average cross-stream velocities are zero outside and inside the bands and no trace of consistent cross-sectional recirculating patterns can be observed

no banding ( $E = 21.3$  V/cm), uniform particle concentration profiles are observed in each layer, as expected. When banding occurs ( $E = 42.6$  V/cm), however, the particles are clearly concentrated in bands in a layer at 6 particle diameters from the wall (orange data in Fig. 6); this concentration along the spanwise direction is however less and less evident moving toward the channel centerline (yellow and purple data) and into regions with lower shear and lower particle concentrations.

As mentioned earlier, combination of shear and electric fields may lead to electrohydrodynamic instabilities in flows with conductivity gradients. Although for the particle volume fractions ( $\phi \approx 0.05\%$ ) that are used in this study, the effect of particles on solution conductivity is negligible (Keh and Ding 2002), the particle accumulation near the channel surfaces may lead to conductivity gradients normal to the surface. To check the existence of counterrotating vortices due to such potential instabilities, which may play a role in the accumulation of particles in the bands, we looked at the average cross-stream velocities  $v_y$  and  $v_z$  versus the spanwise coordinate  $y$  for different layers, corresponding to 0–2, 2–4, and 4–6 particle diameters from the wall (Fig. 7). The velocities are on average always zero inside and outside the bands and no trace of velocity structures that could be associated with cross-stream flows in proximity of the bands are present.

To finalize this section, we show experimental measurements on the transient formation of the bands. In the experiment shown in Fig. 8 (and in the animation in the Online Resource 2), the particle concentrations (and banding formation as well) were measured from the moment when the dc

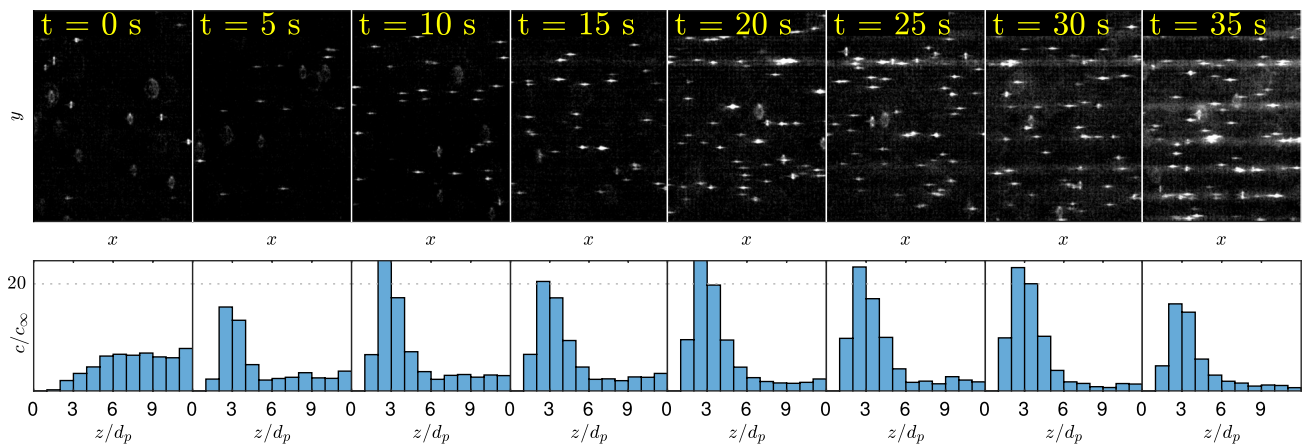


**Fig. 8** Temporal evolution of the particle concentration and band formation (see also Online Resources 2). At  $t = 0$  s, the dc power supply is switched on ( $E = 42.6$  V/cm). Particles start accumulating at the

wall and reach a stable concentration profile after around 20 s. At this point, the band formation starts and stabilizes after around 15 s (35 s after applying the electric field)

power supply was switched on ( $t = 0$  s) until steady-state bands of particles were observed. The whole process took about 35 s for  $E = 42.6$  V/cm. In the first 10 s, the particles accumulate near the wall and no bands are observed. After 10 s, when the concentration profile across the  $z$ -direction becomes steady and the maximum concentration exceeds a volume fraction of 1% (corresponding to  $\approx 20 c_\infty$ ), the bands start forming near the wall. It then takes between 10 and 20 s for the bands to become stable.

## 4 Discussion

*Accumulation/depletion of particles at/from the walls* The experimental results clearly show a robust accumulation of the particles at several particle radii from the wall, which discards any mechanism based on near-wall phenomena involving van der Waals forces (Israelachvili 2011).

Cross-stream “lift” forces experienced by particles in shear flows have been extensively studied both experimentally (Segre and Silberberg 1961; Cherukat and McLaughlin 1994; Matas et al. 2004) and theoretically (Saffman 1965; Cox and Brenner 1968; Ho and Leal 1974; Cherukat and McLaughlin 1994; Zeng et al. 2005; Asmolov et al. 2018) for more than 50 years. This body of work demonstrates that these forces are due to inertial effects, where the flow disturbances created by the difference in particle–fluid inertia interact with the wall (for wall-bounded flows) and/or the nonuniform velocity field in the bulk. Moreover, such a lift force only exists if there is “slip” between the particle and the fluid and the direction of the lift force is determined by the sign of the slip: if particles are slower than the fluid (i.e., lag the flow), they are pushed away, or repelled, from the wall; if particles are faster than the fluid (i.e., lead the flow),

they are pushed towards, or attracted to, the wall. Hence the inertial lift forces on neutrally buoyant particles in shear flows, where particles lag the flow due to their weak retardation near the wall (Goldman et al. 1967a, b), are always repulsive. Attractive forces are possible, however, for (positive or negative) buoyant particles in a vertical channel flow where the sign of the slip can be changed by simply changing the direction of the flow and the density mismatch between the particle and fluid (Jeffrey and Pearson 1965).

Recent experimental studies have revealed that cross-stream lift forces can also be observed in combined pressure and electrokinetically driven flows. Kim and Yoo (2009) used a configuration with positive pressure and voltage drop to concentrate negatively charged colloids in the center of the channels. Similar results have recently been obtained by Yuan et al. (2016) for larger Reynolds numbers, where the electrical field was tuned to obtain attraction/repulsion of particles to/from the channel walls. In both studies, the authors qualitatively attribute the particle migration to an inertial Saffman-like lift, where the direction of the lift (i.e., cross-stream) force depends on whether the particle lags or leads the flow due to its electrophoretic velocity.

Our results confirm that there is a lift force that changes direction depending on the direction of the particle’s electrophoretic velocity (Fig. 9). However, the particle–fluid “slip” in inertial Saffman-like lift is, strictly speaking, due to differences in particle–fluid inertia or density. Nevertheless, recent theoretical studies of inertial migration (Choudhary et al. 2018) suggest that a particle in a combined electroosmotic and Poiseuille flow that leads the flow due to its electrophoretic velocity will migrate toward the region of lower flow velocities (i.e., toward the wall), while a particle that lags the flow migrates toward the region of higher flow velocities (i.e., away from the wall).

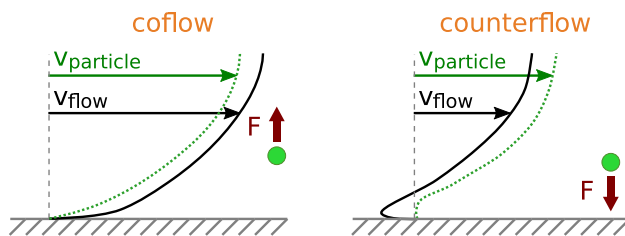


**Fig. 9** Sketch describing the presence of an electrophoretic-induced lift force responsible for the particle migration and its tunability with the direction of the relative pressure/voltage drop

**Particle banding mechanisms** One of the clearest results from our measurements (Fig. 7) is that the flow along the cross-stream directions both normal and parallel to the wall is negligible, which suggests that there are no strong vortices or convection cells sweeping particles into bands. The experimental observations reported above also indicate that particle redistribution, where particles accumulate near the wall and are depleted from the bulk is not solely a near-wall phenomenon. In fact, this redistribution occurs across the entire channel, as would also be expected assuming that the particle flux across any channel cross section is constant.

Additionally, these observations suggest that an accumulation mechanism where the particles are “trapped” in flow stagnation regions is unlikely. Since the electrokinetic flow is very small compared to the Poiseuille flow, the flow stagnation regions are within a particle radius of the wall (e.g., for  $E = 42.6$  V/cm the stagnation point occurs 50 nm from the wall), while the maximum particle concentration is observed at 6 particle radii (3 diameters) from the wall.

The band structures revealed in this study appear to be unique and differ significantly from other structures that are seen in the literature. For instance shear banding phenomena are observed in two-phase systems, in which the two phases tend to separate in regions of high shear (Migler 2001; Caserta et al. 2008) and banding occurs in the region where the highest hydrodynamic shear takes place, i.e., where particle collisions are more likely to occur. Our study, however, differs significantly from shear-banding studies. Shear banding in colloidal solutions has been observed in highly concentrated hard spheres and is characterized by a flow curve of stress versus strain rate, which causes instability and separation into bands with distinct flow velocities (lower particle velocity within the bands compared to the carrying flow) (Besseling et al. 2010). Nonetheless, in our current measurements, we could not observe a significant velocity difference inside and outside the bands (see Fig. 7) and therefore it is unlikely that the origins of the banding phenomenon observed here are analogous to those for classical shear banding.

Similarly, several researchers have shown that particle suspensions under ac electric fields can also generate

band-like structures (Hu et al. 1994; Isambert et al. 1997; Lele et al. 2008; Snoswell et al. 2011). Similar to our observations, particles in these bands appear to be in a disordered liquid-like state; however, unlike our experiments, they generally exhibit chevron patterns. The origins of these structures are attributed to electrohydrodynamic instabilities occurring due to the phase lag between the polarization of the particles and the external ac electric field. Therefore, since only dc electric field is used in the current study, there is no possible analogy with ac electric field banding. More research is therefore required to reveal the mechanisms underlying these phenomena. In particular, many-particle simulations employing different interparticle potentials could investigate whether collective effects could yield the patterns observed here.

## 5 Conclusions

In this work, we have shown that the distribution of suspended colloidal particles in Poiseuille flow in a microfluidic channel with charged walls changes dramatically when a dc electric field, or voltage difference, is applied. When the pressure and the voltage differences are applied in the same direction (coflow), particles are strongly repelled from the wall (Cevheri and Yoda 2014c) and become concentrated in the bulk of the channel. However, when the voltage and pressure differences are applied in opposite directions (counterflow), we have the inverse: the particles accumulate and become concentrated within several particle diameters of the channel walls, and above a minimum electric field magnitude, the particles spontaneously assemble into bands along the flow direction. The bands appear to be stable over extended periods of time ( $\sim 10$  min) and disappear when voltage is turned off with a time scale similar to band formation (see Fig. 8). The bands extend up to 6 particle diameters (as shown in Fig. 6) away from the walls, a distance that corresponds to the maximum particle concentration near the walls (see Fig. 5). We conjecture that the wall-normal migration of the particles is due to inertial “phoretic” lift forces (Choudhary et al. 2018). These forces are fundamentally different from inertial “Saffman-like” lift forces, although they exhibit certain qualitative similarities. We also show that the band formation is more likely due to a collective effect which appears to be correlated with exceeding a particle concentration at least an order of magnitude greater than the bulk value near the wall.

**Acknowledgements** The authors acknowledge financial support by the American National Science Foundation Fluid Dynamics



Program (CBET-1235799) and the Deutsche Forschungsgemeinschaft (KA1808/12 and KA1808/22).

## References

- Anderson JL (1989) Colloid transport by interfacial forces. *Ann Rev Fluid Mech* 21(1):61
- Arca M, Butler JE, Ladd AJ (2015) Transverse migration of polyelectrolytes in microfluidic channels induced by combined shear and electric fields. *Soft Matter* 11(22):4375
- Asmolov ES, Dubov AL, Nizkaya TV, Harting J, Vinogradova OI (2018) Inertial focusing of finite-size particles in microchannels. *J Fluid Mech* 840:613
- Baygents J, Baldessari F (1998) Electrohydrodynamic instability in a thin fluid layer with an electrical conductivity gradient. *Phys Fluids* 10(1):301
- Besseling R, Isa L, Ballesta P, Petekidis G, Cates M, Poon W (2010) Shear banding and flow–concentration coupling in colloidal glasses. *Phys Rev Lett* 105(26):268301
- Bruus H (2008) *Theoretical microfluidics*. Oxford University Press, New York
- Caserta S, Simeone M, Guido S (2008) Shear banding in biphasic liquid–liquid systems. *Phys Rev Lett* 100(13):137801
- Cevheri N, Yoda M (2013) Evanescent-wave particle velocimetry measurements of zeta-potentials in fused-silica microchannels. *Electrophoresis* 34(13):1950
- Cevheri N, Yoda M (2014a) Using shear and direct current electric fields to manipulate and self-assemble dielectric particles on microchannel walls. *J Nanotechnol Eng Med* 5(3):031009
- Cevheri N, Yoda M (2014b) Electrokinetically driven reversible banding of colloidal particles near the wall. *Lab Chip* 14(8):1391–1394
- Cevheri N, Yoda M (2014c) Lift forces on colloidal particles in combined electroosmotic and Poiseuille flow. *Langmuir* 30(46):13771
- Chang MH, Ruo AC, Chen F (2009) Electrohydrodynamic instability in a horizontal fluid layer with electrical conductivity gradient subject to a weak shear flow. *J Fluid Mech* 634:191
- Cherukat P, McLaughlin JB (1994) The inertial lift on a rigid sphere in a linear shear flow field near a flat wall. *J Fluid Mech* 263:1
- Choudhary A, Renganathan T, Renganathan S (2018) *Bulletin of the American Physical Society, Division of Fluid Dynamics* (G24.00009)
- Cierpka C, Segura R, Hain R, Kähler CJ (2010a) A simple single camera 3C3D velocity measurement technique without errors due to depth of correlation and spatial averaging for microfluidics. *Meas Sci Technol* 21(4):045401
- Cierpka C, Rossi M, Segura R, Kähler CJ (2010b) On the calibration of astigmatism particle tracking velocimetry for microflows. *Meas Sci Technol* 22(1):015401
- Cox R, Brenner H (1968) The lateral migration of solid particles in Poiseuille flow-I theory. *Chem Eng Sci* 23(2):147
- Goldman AJ, Cox RG, Brenner H (1967a) Slow viscous motion of a sphere parallel to a plane wall-I motion through a quiescent fluid. *Chem Eng Sci* 22(4):637
- Goldman A, Cox R, Brenner H (1967b) Slow viscous motion of a sphere parallel to a plane wall-II Couette flow. *Chem Eng Sci* 22(4):653
- Ho B, Leal L (1974) Inertial migration of rigid spheres in two-dimensional unidirectional flows. *J Fluid Mech* 65(2):365
- Hu Y, Glass J, Griffith A, Fraden S (1994) Observation and simulation of electrohydrodynamic instabilities in aqueous colloidal suspensions. *J Chem Phys* 100(6):4674
- Isambert H, Ajdari A, Viovy JL, Prost J (1997) Electrohydrodynamic patterns in charged colloidal solutions. *Phys Rev Lett* 78(5):971
- Israelachvili JN (2011) *Intermolecular and surface forces*. Academic Press, Cambridge
- Jeffrey RC, Pearson J (1965) Particle motion in laminar vertical tube flow. *J Fluid Mech* 22(4):721
- Keh HJ, Ding JM (2002) Electrophoretic mobility and electric conductivity of suspensions of charge-regulating colloidal spheres. *Langmuir* 18(12):4572
- Kim YW, Yoo JY (2009) Axisymmetric flow focusing of particles in a single microchannel. *Lab Chip* 9:1043
- Kirby BJ, Hasselbrink EF (2004) Zeta potential of microfluidic substrates: 1 theory, experimental techniques, and effects on separations. *Electrophoresis* 25(2):187
- Lele PP, Mittal M, Furst EM (2008) Anomalous particle rotation and resulting microstructure of colloids in AC electric fields. *Langmuir* 24(22):12842
- Li D, Xuan X (2018) Electrophoretic slip-tuned particle migration in microchannel viscoelastic fluid flows. *Phys Rev Fluids* 3:074202
- Lyklema J (1991) *Fundamentals of interface and colloid science. Volume I: fundamentals*. Elsevier, Amsterdam
- Manz A, Effenhauser CS, Burggraf N, Harrison DJ, Seiler K, Fluri K (1994) Electroosmotic pumping and electrophoretic separations for miniaturized chemical analysis systems. *J Micromech Microeng* 4(4):257
- Matas JP, Morris JF, Guazzelli É (2004) Inertial migration of rigid spherical particles in Poiseuille flow. *J Fluid Mech* 515:171
- Migler KB (2001) String formation in sheared polymer blends: coalescence, breakup, and finite size effects. *Phys Rev Lett* 86(6):1023
- Navaneetham G, Posner JD (2009) Electrokinetic instabilities of non-dilute colloidal suspensions. *J Fluid Mech* 619:331
- Rossi M, Kähler CJ (2014) Optimization of astigmatic particle tracking velocimeters. *Exp Fluids* 55(9):1809
- Russel WB, Saville DA, Schowalter WR (1989) *Colloidal dispersions*. Cambridge University Press, Cambridge
- Sadr R, Yoda M, Zheng Z, Conlisk A (2004) An experimental study of electro-osmotic flow in rectangular microchannels. *J Fluid Mech* 506:357
- Saffman P (1965) The lift on a small sphere in a slow shear flow. *J Fluid Mech* 22(2):385
- Schasfoort RB (1999) Field-effect flow control for microfabricated fluidic networks. *Science* 286(5441):942
- Segre G, Silberberg A (1961) Radial particle displacements in Poiseuille flow of suspensions. *Nature* 189(4760):209
- Snoswell DR, Creaton P, Finlayson CE, Vincent B (2011) Electrically induced colloidal clusters for generating shear mixing and visualizing flow in microchannels. *Langmuir* 27(21):12815
- Yariv E (2006) “Force-free” electrophoresis? *Phys Fluids* 18(3):031702
- Yee A, Yoda M (2018) Experimental observations of bands of suspended colloidal particles subject to shear flow and steady electric field. *Microfluidics Nanofluidics* 22(10):113
- Yuan D, Pan C, Zhang J, Yan S, Zhao Q, Alici G, Li W (2016) Tunable particle focusing in a straight channel with symmetric semicircle obstacle arrays using electrophoresis-modified inertial effects. *Micromachines* 7(11):195
- Zeng L, Balachandar S, Fischer P (2005) Wall-induced forces on a rigid sphere at finite Reynolds number. *J Fluid Mech* 536:1

**Publisher's Note** Springer Nature remains neutral with regard to jurisdictional claims in published maps and institutional affiliations.